Nanoscale Advances

ROYAL SOCIETY OF CHEMISTRY

PAPER

View Article Online
View Journal | View Issue

Cite this: *Nanoscale Adv.*, 2024, **6**, 4434

Unraveling the impact of different liposomal formulations on the plasma protein corona composition might give hints on the targeting capability of nanoparticles†

Esther Imperlini,‡[a] Luisa Di Marzio, ‡[b] Armando Cevenini,[cd] Michele Costanzo, [cd] Nicola d'Avanzo, [ef] Massimo Fresta, [fg] Stefania Orrù,*[dh] Christian Celia *[bijk] and Francesco Salvatore *[cd]

Nanoparticles (NPs) interact with biological fluids after being injected into the bloodstream. The interactions between NPs and plasma proteins at the nano-bio interface affect their biopharmaceutical properties and distribution in the organ and tissues due to protein corona (PrC) composition, and in turn, modification of the resulting targeting capability. Moreover, lipid and polymer NPs, at their interface, affect the composition of PrC and the relative adsorption and abundance of specific proteins. To investigate this latter aspect, we synthesized and characterized different liposomal formulations (LFs) with lipids and polymer-conjugated lipids at different molar ratios, having different sizes, size distributions and surface charges. The PrC composition of various designed LFs was evaluated *ex vivo* in human plasma by label-free quantitative proteomics. We also correlated the relative abundance of identified specific proteins in the coronas of the different LFs with their physicochemical properties (size, PDI, zeta potential). The evaluation of outputs from different bioinformatic tools discovered protein clusters allowing to highlight: (i) common as well as the unique species for the various formulations; (ii) correlation between each identified PrC and the physicochemical properties of LFs; (iii) some preferential binding determined by physicochemical properties of LFs; (iv) occurrence of formulation-specific protein patterns in PrC. Investigating specific clusters in PrC will help decode the multivalent roles of the protein pattern components in the drug delivery process, taking advantage of the bio-nanoscale recognition and identification for significant advances in nanomedicine.

Received 24th April 2024
Accepted 27th June 2024

DOI: 10.1039/d4na00345d

rsc.li/nanoscale-advances

1. Introduction

Liposomes are versatile, biocompatible, biodegradable, low toxic and poorly immunogenic drug delivery systems, which are able to encapsulate both hydrophilic and lipophilic compounds and enhance tumor targeting.[1,2] Lipid composition, average size, surface charge and shape affect biopharmaceutical properties of liposomes as well as their biodistribution and targeting.[3–7] Liposomal formulations (LFs) can improve the safety and efficiency of therapeutics by (i) reducing systemic side effects, (ii) preventing early degradation of payloads, and (iii) targeting specific cells and tissues.[8,9]

[a]*Department for Innovation in Biological, Agrofood and Forest Systems, University of Tuscia, Viterbo, 01100, Italy*

[b]*Department of Pharmacy, University of Chieti – Pescara "G. d'Annunzio", Via dei Vestini 31, 66100, Chieti, Italy. E-mail: c.celia@unich.it; Tel: +39 0871 3554711*

[c]*Department of Molecular Medicine and Medical Biotechnology, School of Medicine, University of Naples Federico II, Naples, 80131, Italy. E-mail: salvator@unina.it; Tel: +39 3356069177*

[d]*CEINGE-Biotecnologie Avanzate Franco Salvatore, Naples, 80145, Italy. E-mail: stefania.orru@uniparthenope.it; Tel: +39 081 3737880*

[e]*Department of Experimental and Clinical Medicine, University of Catanzaro "Magna Graecia", Viale "S. Venuta", 88100, Catanzaro, Italy*

[f]*Department of Experimental and Clinical Medicine, Research Center "ProHealth Translational Hub", "Magna Graecia" University of Catanzaro, Campus Universitario "S. Venuta"—Building of BioSciences, Viale S. Venuta, 88100, Catanzaro, Italy*

[g]*Department of Health Sciences, University of Catanzaro "Magna Graecia", Viale "S. Venuta", 88100, Catanzaro, Italy*

[h]*Department of Medical, Movement and Wellness Sciences, University of Naples Parthenope, Naples, 80133, Italy*

[i]*Lithuanian University of Health Sciences, Laboratory of Drug Targets Histopathology, Institute of Cardiology, A. Mickeviciaus g. 9, LT-44307, Kaunas, Lithuania*

[j]*Institute of Nanochemistry and Nanobiology, School of Environmental and Chemical Engineering, Shanghai University, Shanghai 200444, China*

[k]*UdA-TechLab, Research Center, University of Chieti-Pescara "G. D'Annunzio", 66100, Chieti, Italy*

† Electronic supplementary information (ESI) available. See DOI: https://doi.org/10.1039/d4na00345d

‡ These authors equally contributed.

The incorporation of polyethylene glycol (PEG) polymers into the liposome bilayer (PEGylation) or the modification of the surface properties with other polymeric macromolecules (or surfactants) extend liposomal blood circulation and decrease the clearance mediated by the mononuclear phagocyte system (MPS), hence avoiding their accumulation in the liver and spleen.[10]

MPS activation is triggered by the opsonization process, which is involved in the neutralization of non-self-antigens[11] and is able to reduce liposome biodistribution and circulation half-life.[12] In this scenario, PEGylation of liposomes has long been considered an efficient anti-opsonization strategy to improve long circulation and passive targeting of nanoparticles (NPs).[13,14]

PEG has been widely used to improve the stability and stealth properties of liposomes as well as other lipid-based nanocarriers. To date, PEG with a molecular weight of 2 kDa is currently used to make liposomes that are used in the clinic, such as Doxil® and Onivyde®, and more recently siRNA/mRNA-loaded lipid nanoparticles, such as Onpattro® and Comirnaty®.[15]

However, recent studies demonstrated that PEG polymers, at medium and high molecular weights, conjugated with therapeutics, can activate complement cascades and the relative immune system mediators after multiple systemic injections;[16] on the other hand, they cannot completely prevent the adsorption of plasma proteins on the liposome surface, thus allowing the formation of a coating called protein corona (PrC).[12,17,18]

PrC formation depends on the high free energy of the NP surface, which by interacting with biological fluid components, is coated by various macromolecules, like proteins but also lipids.[18,19] The composition of PrC depends on the intrinsic NP properties, such as the material, size, shape and surface charge.[18,20] The amount of adsorbed proteins is positively correlated with NP size and depends on the curvature of NPs; in fact, the largest particles have a smaller surface bend that allows the proteins to interact more freely with a greater surface area.[21]

PrC formation determines a new biological complex, namely the PrC-NP, with a dynamic structure ruled by affinity interactions (proteins/NP surface, protein/protein).[22] At the nano-bio interface, plasma proteins are continuously desorbed and adsorbed on the NP surface according to the "Vroman effect".[23] In particular, the most tightly bound layer of proteins, the so-called "hard corona",[24] seems to play a fundamental role in the biological interactions of NPs and in the recognition of PrC-NP complexes with the target tissue.[25] In fact, PrC affects the biodistribution of NPs since the plasma proteins show different affinities for different tissues, thus representing an example of active natural targeting.[22,26] As a consequence, PrC is also instrumental in the pharmacokinetics of NPs and their delivered payloads.[11]

PrC composition plays a key role in the stability of the NPs by inducing or preventing their aggregation, together with the NP surface charge and steric hindrances of interacting NPs.[27,28] This knowledge is pivotal to rationally design NPs of different charges and/or steric hindrances whose specific PrC composition could determine, in turn, a specific distribution *in vivo*.[29]

Macromolecule-conjugated lipids like ganglioside-monosialic acid (GM1), with stealth properties and low immune responses at specific molar ratios and molecular weight,[30,31] allow a prolonged circulation of NPs and prevent their MPS uptake and clearance from the bloodstream equal to PEG-phospholipids.[32] Sialic acid residues of GM1 and the oligosaccharide residues conjugated to ceramide lipids have different structures and flexibility[33] compared to polyethylene oxide units of PEG. Differences in the backbone structure of macromolecule-conjugated lipids provide different binding affinity and interactions with circulating proteins that are adsorbed on the NP surface, thereby changing its features although the stealth properties are maintained.[34] These properties further affect the circulation time of NPs after systemic injection, and thus, their clinical outcomes.[35]

In this scenario, LFs represent a versatile class of drug delivery systems able to address new therapeutic opportunities, as mentioned above. Hence, we designed and characterized five different LFs containing: (i) anionic phospholipids (LF1 and LF2); (ii) anionic phospholipids and PEGylated lipids (LF3 and LF4); (iii) anionic phospholipids and GM1 glycolipids (LF5). Each of them was extruded at two different sizes, thus resulting in ten different LFs to be investigated. After incubation in human plasma (HuP), we profiled their PrC composition to study the impact of the variety of chemical and biological moieties at the nano-bio interfaces of NPs. This formulation/size-based multiplexed mapping allowed us to identify specific protein patterns possibly instrumental for interaction with diverse biological tissues.[36,37] The combined data from PrC profiling and physicochemical characterization of liposomes can be used as an effective approach to obtain NPs with optimal properties for their specific purpose.

2. Methods

2.1. Chemical and reagents

1,2-Dipalmitoyl-*sn-glycero*-3-phosphocholine monohydrate (DPPC), 1,2-dipalmitoyl-*sn-glycero*-3(phospho-L-serine), sodium salt (DPPS), 1,2-dimyristoyl-*sn-glycero*-3-phospho-(1-rac-glycerol), sodium salt (DMPG), 1,2-distearoyl-*sn-glycero*-3-phosphoethanolamine-*N*-[methoxy(polyethylene-glycol)-750], ammonium salt (DSPEmPEG750), 1,2-distearoyl-*sn-glycero*-3-phosphoethanolamine-*N*-[methoxy(polyethylene-glycol)-5000], ammonium salt (DSPEmPEG5000), ganglioside, brain, ovine–sodium salt (GM1) and cholesterol (Chol) were obtained from Avanti® Polar Lipids (Alabaster, AL, USA).

N-2-Hydroxyethylpiperazine-*N*-2-ethanesulfonic acid (HEPES), Whatman filters, DL-dithiothreitol minimum 99% titration, modified trypsin, Laemmli buffer, dithiothreitol (DTT), iodoacetamide (IAA), and ammonium bicarbonate (AMBIC) were purchased from Sigma Aldrich (Milano, Italy). Gelcode® blue stain reagent was obtained from Thermo Fisher Scientific (Waltham, MA, US). Tris–HCl, sodium dodecyl sulfate (SDS), acrylamide, bis-acrylamide, ammonium persulfate (APS), tetramethylethylenediamine (TEMED), tris/glycine/SDS (TGS)

and tris/glycine (TG) buffers were obtained from Bio-Rad Laboratories Srl (Segrate, Italy). HPLC grade acetonitrile (ACN) and formic acid were purchased from J. T. Baker (Deventer, Netherlands).

2.2. Liposome preparation

Liposomal formulations (LFs) were prepared by using the thin layer evaporation method and extrusion technique.[38] Briefly, lipids (different molar ratios of DPPC, DPPS, DMPG, DSPE-mPEG750, DSPE-mPEG5000, GM1 and Chol, as reported in Table 1) were dissolved in chloroform/methanol (3 : 1, v/v). Then, the organic solvent was removed by using a rotary evaporator (model Laborota 4000 type Heidolph, Delchimica, Naples, Italy) at 50 °C to remove any solvent residues, and the lipid film was left under the hood overnight at room temperature. The resulting multilamellar liposomes were obtained by hydrating the dried lipid film with HEPES (10 mM, pH = 7.4) and by alternating three cycles of heating at 60 °C and of continuous stirring for 3 min. LFs were extruded by using a Lipex ExtruderTM device (Northern Lipids Inc., BC, Canada) with polycarbonate membranes (Whatman Inc., NJ, USA) having pore sizes of 200 nm and 100 nm. Large LFs (LF-L) and small LFs (LF-S) were collected and used for further experiments.

2.3. Physicochemical characterization of liposomes

The average size (nm) (hydrodynamic radius) and polydispersity index (PDI) of LFs were measured by using dynamic light scattering (DLS).[39] Zeta potential (mV) was determined as electrophoretic mobility by laser doppler electrophoresis (LDE). To avoid multi-scattering phenomena, samples were diluted (1 : 30 v/v) in HEPES (10 mM, pH = 7.4) and then analyzed by using Zetasizer Nano ZS90 (Malvern Panalytical, United Kingdom). Measurements were performed in three different replicates; each of them was repeated at least five times, and data were reported as average ± standard deviation (SD).

2.4. Human plasma preparations and incubation with liposomes

Human plasma (HuP) samples were obtained at CEINGE – Biotecnologie Avanzate Franco Salvatore (Naples, Italy) from healthy adult volunteers (30–50 years) in accordance with the relevant laws and guidelines existing in Italy with the declaration of Helsinki. Informed consents were obtained from human participants (blood plasma donors) of this study, and the experiments were performed in accordance with the guidelines of the declaration of Helsinki and approved by the Ethics Committee of the University of Naples Federico II (approval number 318/20).

Blood samples were collected by using the BDTMP100 Blood Collection System in the presence of K_2EDTA anticoagulant and protease inhibitor cocktail. HuP samples were prepared as previously reported.[18] Briefly, after clot formation, HuP was collected by centrifugation at 1000*g* for 5 min.

To reduce inter-individual variations, we pooled HuP samples from the different donors and stored their aliquots at −80 °C. Afterwards, HuP aliquots were thawed at 4 °C and warmed at room temperature.

The HuP samples were incubated (1 : 1, v/v) with LFs (10 mg ml^{-1}) at 37 °C for 1 h. After incubation, PrC-NP complexes were isolated by centrifugation at 15 000*g* for 10 min and washed with PBS twice. At each washing step, samples were transferred into new Protein LoBind tubes and then resuspended in Laemmli buffer.

2.5. Protein corona electrophoresis and in-gel digestion

Proteins suspended in Laemmli buffer were first denatured at 95 °C for 5 min and then fractionated by 12% (v/v) SDS-PAGE. The protein bands were stained using Gelcode® blue stain reagent (Thermo Fisher Scientific, USA) according to the manufacturing procedures. Molecular weights (MW) of protein bands were estimated by using Precision Plus All Blue protein standards (Bio-Rad). The gel image was acquired using the scanner GS-800 Calibrated Densitometer (Bio-Rad).

The whole gel lanes were manually cut into 2 mm gel slices. Each slice was washed with ACN and 50 mM AMBIC as previously reported.[40] The protein bands were then reduced with 10 mM DTT in 50 mM AMBIC at 56 °C for 45 min and then alkylated in 55 mM IAA in 50 mM AMBIC at room temperature, in the dark for 30 min. After washing with ACN and 50 mM AMBIC, each slice was incubated with 10 ng μL^{-1} trypsin at 4 °C as previously described.[41] Peptide mixtures were extracted and resuspended in 0.2% (v/v) formic acid.

Table 1 Different molar ratios of phospholipids and cholesterol constituting the liposomal formulations (LFs). The numerical figures indicate the molar ratio of components in each formulation

LFs	DPPC[a]	DPPS[b]	DMPG[c]	DSPE-mPEG750[d]	DSPE-mPEG5000[e]	GM1[f]	CHOL[g]
LF1	6	1	—	—	—	—	3
LF2	6	—	1	—	—	—	3
LF3	6	—	—	1	—	—	3
LF4	6	—	—	—	1	—	3
LF5	6	—	—	—	—	0.5	3.5

[a] 1,2-Dipalmitoyl-*sn-glycero*-3-phosphocholine monohydrate. [b] 1,2-Dipalmitoyl-*sn-glycero*-3(phospho-L-serine). [c] 1,2-Dimyristoyl-*sn-glycero*-3-phospho-(1-rac-glycerol). [d] 1,2-Distearoyl-*sn-glycero*-3-phosphoethanolamine-*N*-[methoxy(polyethylene-glycol)-750]; 750 is low-MW PEG. [e] 1,2-Distearoyl-*sn-glycero*-3-phosphoethanolamine-*N*-[methoxy(polyethylene-glycol)-5000]; 5000 is high-MW PEG. [f] Monosialotetrahexosylganglioside. [g] Cholesterol.

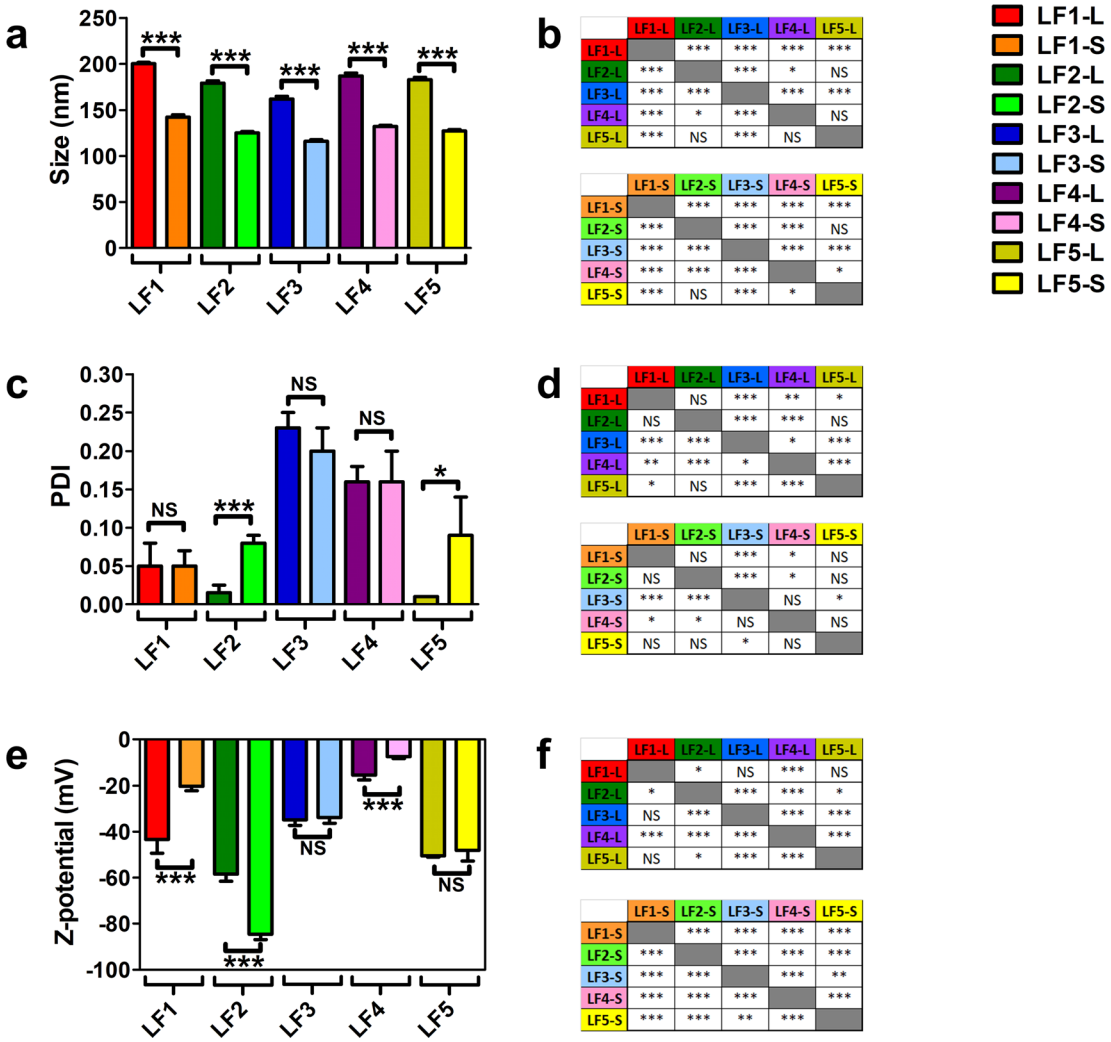

Fig. 1 Dynamic light scattering (DLS) and laser doppler electrophoresis (LDE) analyses of LFs. LFs were produced using five different compositions, as reported in Table 1. For each composition, the vesicles were extruded at two different sizes through polycarbonate filters with large (200 nm) and small (100 nm) pore size membrane filters, thus finally obtaining ten different LFs. LFs extruded through 200 nm and 100 nm pore-size membrane filters were named LF-L and LF-S, respectively. (a) Measurements of average size (nm), (c) polydispersity index (PDI) and (e) zeta potential (mV) of different bare LFs. Results are the mean of three different replicates for which five technical repeats were considered and data were expressed as average ± SD. (b, d and f) Statistical significance was calculated by one-way *T*-test for each pairwise comparison among the LFs for the differences in average size, PDI and Z-potential, respectively. * = p value < 0.05; *** = p value < 0.005; NS = not significant.

2.6. LC-MS/MS analysis for protein identification and quantification

Protein identification was carried out using a liquid chromatography-tandem mass spectrometry (LC-MS/MS)-based proteomics pipeline.[42,43] LC-MS/MS analyses were performed using the LC/MSD Trap XCT Ultra (Agilent Technologies, Palo Alto, CA) equipped with a 1100 HPLC system and a chip cube (Agilent Technologies) as previously described.[44]

Raw MS/MS data files were submitted to Mascot software (Matrix Science, UK) for protein identification.[45] Precisely, the following search parameters were applied: NCBI as protein database; trypsin as specific proteolytic enzyme; *Homo sapiens* as taxonomy; one missed cleavage; *S*-carbamidomethyl cysteine as fixed modification; oxidized methionine and N-terminal pyroglutamic as variable modifications; 300 ppm and 0.6 Da as mass tolerance on precursor ions and product ions, respectively. Finally, a Mascot individual ion score >43 was considered for an unambiguous data interpretation (p value <0.05).

The mass spectrometry proteomics data have been deposited to the ProteomeXchange Consortium *via* the PRIDE partner repository[46] with the dataset identifier PXD052701.

Quantitative analysis of LC-MS/MS data was performed by label-free quantification, subjecting the Mascot format text files to Proteome Discoverer v1.4 (Thermo Fisher Scientific, USA). Spectral count (SpC) values and Normalized Spectral Abundance Factor (NSAF) were used as quantitative parameters for estimating protein abundance.[47] Briefly, the SpC of each protein was divided by its length, defining the spectral abundance factor (SAF), and normalized to the total sum of SpC in a given lane, obtaining the Normalized Spectral Abundance Factor

Table 2 Relative abundance of PrC components identified in at least eight out of ten LFs is expressed as normalized spectral abundance factor (NSAF)

Gene	NSAF LF1-S	NSAF LF1-L	NSAF LF2-S	NSAF LF2-L	NSAF LF3-S	NSAF LF3-L	NSAF LF4-S	NSAF LF4-L	NSAF LF5-S	NSAF LF5-L
FCN3	9.1%	6.3%	2.7%	0.8%	4.4%	3.5%	6.1%	5.4%	5.7%	4.8%
ALB	13.2%	15.9%	24.5%	20.3%	26.5%	23.9%	7.9%	12.4%	20.2%	25.1%
F5	1.3%	3.7%	1.5%	1.2%	0.7%	0.4%	1.1%	0.8%	0.1%	0.5%
VTN	1.2%	2.0%	0.7%	1.6%	0.6%	0.8%	1.2%	1.2%	0.4%	0.5%
SERPINA1	1.4%	1.4%	2.2%	1.7%	1.9%	1.9%	0.9%	1.1%	1.8%	1.4%
FGG	0.3%	0.6%	1.3%	0.8%	1.3%	1.5%	0.7%	0.8%	1.0%	2.0%
C1QC	1.2%	2.5%	2.2%	1.0%	1.1%	2.9%	2.9%	2.7%	1.7%	1.2%
IGKC	26.3%	18.7%	19.5%	16.2%	25.1%	19.4%	26.6%	30.8%	33.2%	23.8%
CD5L	2.3%	2.7%	1.5%	0.8%	0.8%	1.3%	1.4%	1.1%	0.4%	0.4%
IGHM	14.2%	13.0%	6.1%	14.4%	6.7%	11.0%	10.8%	14.1%	3.0%	4.5%
SLC4A1	0.4%	1.1%	2.2%	1.3%	1.2%	2.3%	1.7%	0.7%	—	0.1%
C3	0.5%	0.4%	0.8%	0.8%	0.6%	0.3%	—	0.2%	1.3%	0.8%
A2M	0.1%	0.4%	0.8%	0.7%	0.6%	1.0%	—	0.1%	1.4%	1.7%
APOA1	2.3%	2.6%	0.9%	1.4%	1.0%	1.9%	0.6%	—	1.9%	0.7%
C1QB	2.8%	3.5%	—	1.1%	1.8%	0.7%	4.9%	0.7%	1.6%	1.3%
C1QA	1.2%	0.9%	0.3%	0.7%	1.1%	0.7%	1.3%	0.4%	—	—
HP	1.2%	1.5%	1.5%	0.7%	1.5%	0.8%	—	—	0.7%	2.2%
TF	0.8%	0.9%	1.4%	1.4%	1.2%	0.5%	—	—	1.1%	1.3%
FGA	0.2%	0.1%	0.1%	—	0.2%	0.2%	0.2%	0.7%	—	0.1%
IGLC2	—	—	5.0%	5.1%	7.3%	3.8%	7.6%	2.7%	10.0%	7.8%
IGHG2	—	—	10.2%	13.3%	7.7%	8.7%	13.8%	9.5%	4.2%	7.5%
IGHA1	—	—	1.4%	2.3%	1.0%	1.5%	2.3%	1.6%	1.2%	0.3%

(NSAF). To compare the expression of the same protein between different LFs, the log ratio of SpC (R_{sc}) was calculated as previously reported.[40]

2.7. Bioinformatics analysis

The identified proteins were classified according to the Database for Annotation, Visualization and Integrated Discovery (DAVID) v6.8 (https://www.david.abcc.ncifcrf.gov/).[48] Based on Fisher's exact test, the DAVID tool can measure the protein enrichment in Gene Ontology (GO) annotation terms (p-value $\leq$0.05). In addition, the Search Tool for the Retrieval of Interacting Genes (STRING) v11 (https://www.string-db.org/) was used to analyze the most statistically significant and non-redundant biological processes among the differentially represented proteins from the label-free proteomic analysis.[49] Only annotations of biological processes with a false discovery rate (FDR) $\leq$0.05 are considered significant.

Proteome data were further analyzed using Perseus software v1.6.15.0 for hierarchical clustering through heatmap visualization and profile plot analysis.[50,51] All the clustering analyses were carried out by choosing Euclidean distance and preprocessing with the k-means algorithm, allowing spontaneous grouping without preserving sample order. Moreover, STRING or the STRINGapp through Cytoscape v3.9 software was also used to build protein–protein interaction (PPI) networks for the proteins of interest.[52,53]

3. Results and discussion

Nanotechnology and proteomics coupled with bioinformatics have been implemented to investigate the biological effect of PrC adsorbed on different multicomponent LFs, and hence, to shed light on their possible ability to target specific tissues.

3.1. Physicochemical characteristics of liposomes with different formulations

Liposomes, with different lipid compositions, were studied to evaluate the effect of the net charge of phospholipid polar head groups and the surface properties of nanocarriers on the protein corona adsorption and composition. PrC composition mainly depends on liposome surface properties, although payload drug molecules can further affect these properties.[54] Currently, PEG is the gold standard polymer that confers long-circulating properties to liposomes.[55] However, evidence showed that PEG activates the immune system after multiple injections,[56] and alternative PEG-like polymers with stealth properties are needed for systemic injection to avoid the immune system activation by liposomes. In this scenario, gangliosides such as GM1 represent a suitable alternative to PEG owing to their stealth properties, stability in biological fluids, and immune system avoidance.[16] GM1 was recently used as a neuroprotective agent for the treatment of brain disorders,[57,58] and GM1-liposomes are currently in phase I clinical trial for the treatment of Parkinson's disease.[59] We recently demonstrated that GM1-liposomes are stable in human plasma and like PEGylated liposomes, long-circulate after systemic injection in murine models and decrease neuronal inflammation and stroke in animal models.[60]

Given such premises, five liposomal formulations (from LF1 to LF5) were synthetized by self-assembling different molar ratios of some lipids (DPPC, DPPS, DMPG, DSPE-mPEG750, DSPE-mPEG5000, GM1) and cholesterol, as shown in Table 1. All LFs contained zwitterionic DPPC, whose safe nature and low

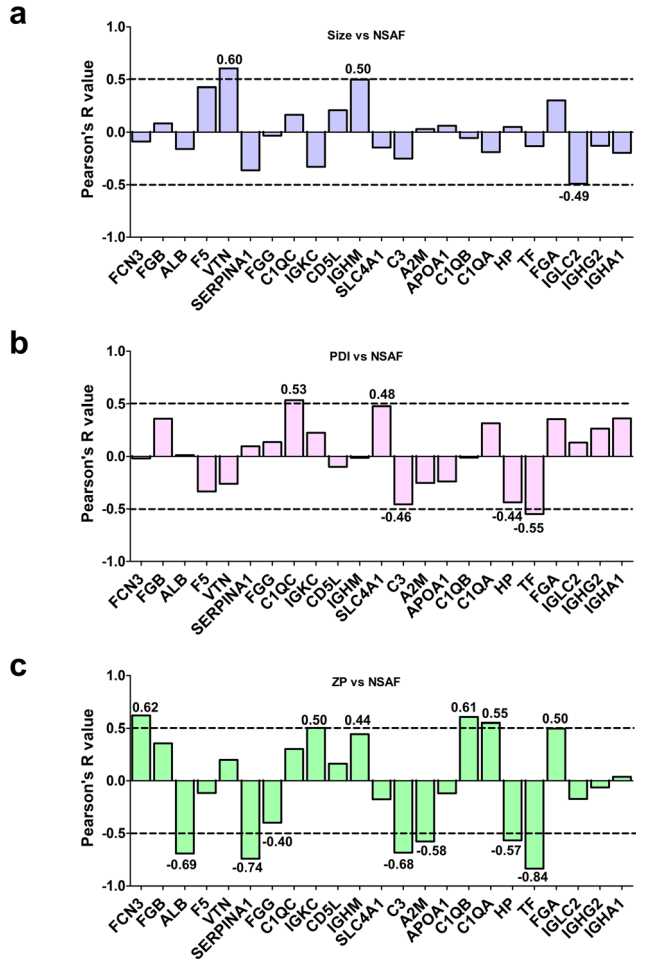

Fig. 2 Correlation between the relative abundance of PrC components and physicochemical properties of LFs. Protein abundance based on MS spectral counts was correlated with (a) the average size, (b) PDI and (c) zeta potential of bare LFs by calculating Pearson's coefficients. The proteins are reported with the names/acronyms of their coding genes.

immunogenic properties make the liposomes suitable for nanomedicine applications. LFs designed for this study contained: (i) anionic phospholipids (LF1 and LF2);[61] (ii) anionic phospholipids and PEGylated lipids (LF3 and LF4); (iii) anionic phospholipids and GM1 glycolipids (LF5). Each LF was extruded through polycarbonate filters with large (200 nm; LF-L) and small (100 nm; LF-S) pore sizes, thus obtaining a total of 10 formulations.

All these formulations were characterized by using DLS and LDE analyses; average size, polydispersity (PDI) and zeta potential of bare LFs were used as references for their physicochemical characterization. As reported in Fig. 1a, the average size of all bare LFs was in the range from 116.0 ± 1.8 nm to 200.1 ± 1.5 nm. LF1 showed the highest average size among all LFs (p value < 0.005, Fig. 1b). Conversely, the average size of LF3 was the smallest of all LFs-L and LFs-S, respectively (p value < 0.005, Fig. 1b). Among PEG-coating formulations, LF4 showed significantly increased average size compared to LF3 (p value < 0.005, Fig. 1b). These results could depend on the different MW of PEG chains bound to DSPE in LF4 and LF3 that, by rearranging differently on the liposomal surface, affected the final packing of the liposomal bilayer. In fact, the greater flexibility of high MW PEG compared to low MW PEG might affect the self-assembling of lipid derivatives into the liposomal bilayer.[62,63] Nonetheless, PEG chains (up to 5 kDa MW) conjugated to DSPE have been widely used to synthesize long-circulating liposomes for drug delivery.[64] Only LF5-L showed a similar average size compared to LF4-L with a non-significant difference (Fig. 1b). These results could be explained by the similar spatial distribution and rearrangement of polyethylene oxide chains of DSPE-PEG5000 and monosialotetrahexosyl chains of GM1, and by the amphipathic nature of both macromolecules and their relative steric barrier activity.[65] Moreover, the amphipathic properties of DSPE-PEG5000 and GM1 allow micelle-like structures depending on the binding energy of curvature radius and the self-assembling energy-dependent process.[66,67]

All the LFs showed PDI <0.25, thus suggesting that liposomes were stable with narrow size distribution[68] (Fig. 1c). PEG-containing LFs (LF3 and LF4) showed higher PDI values compared to the others (Fig. 1d), likely because of PEG chains on the liposome structure. Interestingly, by comparing PDI values between large and small LFs, only LF2-L ($p < 0.005$) and LF5-L ($p < 0.05$) showed significant differences compared to their small counterparts. We can speculate that the highest net negative charge of LF2 and LF5, due to DMPG and GM1, generated a diverse charge distribution on their surface, characterized by a significantly different colloidal interface area. Such conditions may change the net curvature radius of liposomes, increasing their final values of PDI after extrusion through polycarbonate membrane at a specific pressure.

The analyses of zeta potential showed negative values for all LFs with a net negative surface charge below −15 mV (Fig. 1e), thus suggesting the synthesis of stable liposomes. LF2 showed the most negative zeta potential compared to all LFs ($p < 0.005$ and $p < 0.05$, Fig. 1f). The MW of PEG affects the zeta potential of LF3 and LF4, with LF3 more negatively charged than LF4 (Fig. 1f). Differences in the zeta potential values can depend on the number of polyethylene oxide chains that are present in the backbone structure of DSPE-PEG5000 and DSPE-PEG750, suggesting that low MW PEG has a lower shielding capability than high MW PEG.[69] Different from PEG, GM1 had a lower shielding effect on LF5 (Fig. 1e). Finally, all LFs, except for LF3 and LF5, also showed statistically significant differences among LFs-L *versus* LFs-S ($p < 0.005$, Fig. 1e).

3.2. Quali-quantitative composition of liposome PrC and correlations with LF physicochemical properties

HuP was incubated with LFs to allow the formation of PrC-NP complexes. After the elution from LFs, adsorbed HuP proteins were separated by SDS-PAGE (ESI Fig. S1†), and the bands were analyzed by LC-MS/MS for protein identification. The PrC components associated with each LF (from LF1 to LF5) are listed in ESI Tables S1–S5,† including the details of MS analysis.

We identified a total of 72 unique proteins adsorbed on and shared by the different LFs; in particular, MS analysis assigned

Table 3 Functional annotation analysis of PrC identified components adsorbed on liposomal formulations extruded at 200 nm and 100 nm (LFs-L and LFs-S, respectively)

LFs	LF GO terms	Functional categories	*p*-Value	Proteins
LF1-L	Immunoglobulin receptor binding	MF[a]	3.5×10^{-7}	IGHA2, IGHG3, IGHM, IGKC, IGJ
	Fibrinogen complex	CC[b]	7.5×10^{-7}	FGA, FGB, FGG, THBS1
	Protein polymerization	BP[c]	3.2×10^{-6}	FGA, FGB, FGG, VTN
LF1-S	Immunoglobulin receptor binding	MF[a]	1.7×10^{-7}	IGHA2, IGHG3, IGHM, IGKC, IGJ
	Protein polymerization	BP[c]	1.9×10^{-6}	FGA, FGB, FGG, VTN
	Fibrinogen complex	CC[b]	1.1×10^{-4}	FGA, FGB, FGG
	Very-low-density lipoprotein particle	CC[b]	5.9×10^{-4}	APOB, APOE, APOA1
LF2-L	Complement activation	BP[c]	6.8×10^{-13}	C1QA, C1QB, C1QC, C3, C4A, CFB, FCN3, IGHG2, IGKC, IGLC2
	Immunoglobulin receptor binding	MF[a]	4.2×10^{-9}	IGHA1, IGHG2, IGHM, IGKC, IGLC2, IGJ
	Fibrinogen complex	CC[b]	1.8×10^{-4}	FGB, FGG, THBS1
	Very-low-density lipoprotein particle	CC[b]	9.6×10^{-4}	APOA1, APOE, APOL1
LF2-S	Immunoglobulin receptor binding	MF[a]	2.8×10^{-9}	IGHA1, IGHG2, IGHM, IGKC, IGLC2, IGJ
	Protein polymerization	BP[c]	3.0×10^{-6}	FGA, FGB, FGG, VTN
LF3-L	Immunoglobulin receptor binding	MF[a]	6.7×10^{-9}	IGHA1, IGHG2, IGHM, IGKC, IGLC2, IGJ
	Fibrinogen complex	CC[b]	1.2×10^{-6}	FGA, FGB, FGG, THBS1
LF3-S	Immunoglobulin receptor binding	MF[a]	3.6×10^{-9}	IGHA1, IGHG2, IGHM, IGKC, IGLC2, IGJ
	Fibrinogen complex	CC[b]	8.1×10^{-7}	FGA, FGB, FGG, THBS1
LF4-L	Immunoglobulin receptor binding	MF[a]	2.6×10^{-8}	IGHA1, IGHG2, IGHM, IGKC, IGLC2
	Protein polymerization	BP[c]	5.5×10^{-7}	FGA, FGB, FGG, VTN
LF4-S	Immunoglobulin receptor binding	MF[a]	7.6×10^{-8}	IGHA1, IGHG2, IGHM, IGKC, IGLC2
	Fibrinogen complex	CC[b]	2.7×10^{-7}	FGA, FGB, FGG, THBS1
	Protein polymerization	BP[c]	1.2×10^{-6}	FGA, FGB, FGG, VTN
LF5-L	Phagocytosis, engulfment	BP[c]	2.0×10^{-8}	GSN, IGHA1, IGHG2, IGHM, IGKC, IGLC2
	Fibrinogen complex	CC[b]	8.8×10^{-7}	FGA, FGB, FGG, THBS1
	Protein polymerization	BP[c]	3.8×10^{-6}	FGA, FGB, FGG, VTN
LF5-S	Complement activation	BP[c]	1.3×10^{-14}	C1QB, C1QC, C3, C4A, CFB, FCN2, FCN3, IGHG2, IGKC, IGLC2
	Phagocytosis, engulfment	BP[c]	6.6×10^{-9}	GSN, IGHA1, IGHG2, IGHM, IGKC, IGLC2
	Phosphatidylcholine-sterol *O*-acyltransferase activator activity	MF[a]	5.5×10^{-5}	APOA1, APOA4, APOE
	Protein polymerization	BP[c]	2.9×10^{-4}	FGB, FGG, VTN

[a] Molecular function. [b] Cellular component. [c] Biological process.

36 protein species for LF1-S, 42 for LF1-L, 39 for LF2-S, 43 for LF2-L, 41 for LF3-S, 47 for LF3-L, 29 for LF4-S, 24 for LF4-L, 34 for LF5-S and 43 for LF5-L (ESI Tables S1–S5†). Based on MS spectral counts, the relative abundances of these identified proteins were expressed as normalized spectral abundance factor (NSAF) and then evaluated and compared in all LFs. A total of 23 different proteins identified in the corona of at least eight out of ten LFs are listed in Table 2. Among them, 11 species were found to bind all the LFs with different abundances. Immunoglobulin kappa constant (IGKC) and albumin (ALB) were the most represented species in all formulations, showing 24.0 ± 5.5% and 19.0 ± 6.3% as average abundance, respectively. Some other species had a preferential binding based on the size of a specific LF (for example, band 3 anion transport protein, SLC4A1, for LF5-L) or were undetected in specific formulations, regardless of the size (for example, haptoglobin, HP, and transferrin, TF) for LF4.

The functional/pathway analysis performed on this specific set of proteins revealed that 15 out of 23 clustered in a high-interconnected network related to the "complement and coagulation cascades" pathway (FDR = 8.09×10^{-21}), also including a subnetwork of the complement C1q subunits (C1QA, C1QB and C1QC), (ESI Fig. S2†).

To assess whether the relative abundance of this set of 23 species could be related to their physicochemical properties, we determined the Pearson's coefficients between protein-specific MS spectral counts and the average size, or PDI or zeta potential of the bare LFs (Fig. 2). As shown in Fig. 2a, only vitronectin (VTN) exhibited a significant positive association with the average size of LFs. Interestingly, high levels of VTN were observed in the PrC of lipidic NPs, showing a preferential accumulation in tumor tissues.[70] This finding highlights the importance of VTN-enriched corona on liposomes in terms of their putative capability to target cancer cells over-expressing the integrin receptor.

As for PDI, only C1QC and TF proteins showed significant Pearson's *R* values: C1QC showed a positive association, thus implicating that the higher amount matched more polydisperse liposomes, whereas TF showed a negative correlation, suggesting a binding preference to more homogeneous LFs (Fig. 2b). C1QC is a well-known protein of the C1q family, which carries out an essential role in innate immunity, contributing to nonspecific host defense.[71,72] On the other hand, TF is an

Table 4 Quantitative proteomic analysis of PrC components for LF1-L *versus* LF1-S

Protein	Gene	R_{SC}[a]
Thrombospondin-1	THBS1	4.27
Inter-alpha-trypsin inhibitor heavy chain H4	ITIH4	3.42
Inter-alpha-trypsin inhibitor heavy chain H1	ITIH1	3.21
Inter-alpha-trypsin inhibitor heavy chain H2	ITIH2	2.97
Spectrin beta chain, erythrocytic	SPTB	2.68
Spectrin alpha chain, erythrocytic 1	SPTA1	2.68
Ankyrin-1	ANK1	2.32
Ceruloplasmin	CP	1.83
Coagulation factor V	F5	1.32
Alpha-2-macroglobulin	A2M	1.31
Band 3 anion transport protein	SLC4A1	1.22
Immunoglobulin J chain	IGJ	1.10
Complement C1q subcomponent subunit C	C1QC	0.737
Histidine-rich glycoprotein	HRG	0.645
Vitronectin	VTN	0.458
Fibrinogen gamma chain	FGG	0.441
Clusterin	CLU	0.441
Immunoglobulin alpha-2 heavy chain	IGHA2	0.377
Ig gamma-3 chain C region	IGHG3	0.341
Actin, cytoplasmic 1	ACTB	0.044
Haptoglobin	HP	0.016
Complement C1q subcomponent subunit B	C1QB	−0.001
Serum albumin	ALB	−0.028
CD5 antigen-like	CD5L	−0.087
Apolipoprotein A–I	APOA1	−0.141
Serotransferrin	TF	−0.167
Alpha-1-antitrypsin	SERPINA1	−0.301
Ficolin-2	FCN2	−0.352
Immunoglobulin heavy constant mu	IGHM	−0.484
Fibrinogen alpha chain	FGA	−0.496
Lipopolysaccharide-binding protein	LBP	−0.497
Complement C1q subcomponent subunit A	C1QA	−0.643
Complement C3	C3	−0.667
Immunoglobulin kappa variable 3–15	IGKV3–15	−0.786
Immunoglobulin heavy variable 1–3	IGHV1–3	−0, 786
Immunoglobulin kappa constant	IGKC	−0.826
Ficolin-3	FCN3	−0.875
Apolipoprotein E	APOE	−0.905
Fibrinogen beta chain	FGB	−1.01
C4b-binding protein alpha chain	C4BPA	−1.14
Hemopexin	HPX	−1.39
Vitamin D-binding protein	GC	−1.58
Alpha-1-antichymotrypsin	SERPINA3	−2.37
Apolipoprotein B-100	APOB	−3.30

[a] R_{sc}, log 2 ratio between the protein expression levels in the corona of LF1-L *versus* LF1-S. Proteins in grey with $R_{sc} \geq 1.40$ or ≤ -1.40 were considered differentially represented.

Table 5 Quantitative proteomic analysis of PrC components for LF2-L *versus* LF2-S

Protein	Gene	R_{sc}[a]
Spectrin beta chain, erythrocytic	SPTB	5.08
Alpha-1-acid glycoprotein 1	ORM1	4.42
Complement C1q subcomponent subunit B	C1QB	3.93
Ankyrin-1	ANK1	3.93
Histidine-rich glycoprotein	HRG	3.72
Ceruloplasmin	CP	3.72
Thrombospondin-1	THBS1	3.48
Apolipoprotein L1	APOL1	2.83
C4b-binding protein alpha chain	C4BPA	2.83
Alpha-1B-glycoprotein	A1BG	2.34
Immunoglobulin J chain	IGJ	2.10
Alpha-1-acid glycoprotein 1	ORM1	4.42
Complement C1q subcomponent subunit B	C1QB	3.93
Ankyrin-1	ANK1	3.93
Histidine-rich glycoprotein	HRG	3.72
Ceruloplasmin	CP	3.72
Thrombospondin-1	THBS1	3.48
Apolipoprotein L1	APOL1	2.83
C4b-binding protein alpha chain	C4BPA	2.83
Alpha-1B-glycoprotein	A1BG	2.34
Immunoglobulin J chain	IGJ	2.10
Immunoglobulin heavy constant mu	IGHM	1.39
Vitronectin	VTN	1.23
Complement C1q subcomponent subunit A	C1QA	0.867
Ig alpha-1 chain C region	IGHA1	0.741
Apolipoprotein A–I	APOA1	0.568
Complement factor B	CFB	0.503
Ig gamma-2 chain C region	IGHG2	0.426
Vitamin D-binding protein	GC	0.380
Alpha-1-antichymotrypsin	SERPINA3	0.380
Ig lambda-2 chain C regions	IGLC2	0.016
Spectrin alpha chain, erythrocytic 1	SPTA1	0.016
Complement C4-A	C4A	0.016
Complement C3	C3	−0.028
Serotransferrin	TF	−0.045
Alpha-2-macroglobulin	A2M	−0.091
Inter-alpha-trypsin inhibitor heavy chain H2	ITIH2	−0.226
Inter-alpha-trypsin inhibitor heavy chain H4	ITIH4	−0.226
Immunoglobulin kappa constant	IGKC	−0.273
Peroxiredoxin-2	PRDX2	−0.274
Alpha-1-antitrypsin	SERPINA1	−0.353
Inter-alpha-trypsin inhibitor heavy chain H1	ITIH1	−0.383
Serum albumin	ALB	−0.402
Coagulation factor V	F5	−0.407
Fibrinogen gamma chain	FGG	−0.600
Band 3 anion transport protein	SLC4A1	−0.727
CD5 antigen-like	CD5L	−0.840
Actin, cytoplasmic 1	ACTB	−0.935
Haptoglobin	HP	−1.05
Complement C1q subcomponent subunit C	C1QC	−1.05
Apolipoprotein E	APOE	−1.11
Fibrinogen beta chain	FGB	−1.52
Ficolin-3	FCN3	−1.66
Catalase	CAT	−2.31
Clusterin	CLU	−2.79
Fibrinogen alpha chain	FGA	−2.79
Immunoglobulin heavy variable 3–9	IGHV3	−3.16
Serum amyloid P-component	APCS	−3.45
Ficolin-2	FCN2	−4.24

[a] R_{sc}, log 2 ratio between the protein expression levels in the corona of LF2-L *versus* LF2-S. Proteins in grey with $R_{sc} \geq 1.40$ or ≤ -1.40 were considered differentially represented.

abundant human serum iron-binding glycoprotein with multi-task functions,[73] well known for its natural targeting ability; as a matter of fact, it is used as a ligand for functionalizing NPs to actively target brain[74] and/or cancer cells.[75,76]

Interestingly, we found several significant correlations between the protein relative abundances of PrC components and zeta potential (Fig. 2c). Indeed, ficolin-3 (FCN3), C1QA and C1QB were positively associated, thus implicating that their preferred binding was toward the less negative NPs. On the other hand, the relative abundances of ALB, alpha-1-antitrypsin (SERPINA1), complement C3 (C3), alpha-2-macroglobulin (A2M), HP and TF were negatively associated with zeta

Table 6 Quantitative proteomic analysis of PrC components for LF3-L *versus* LF3-S

Protein	Gene	R_{sc}[a]
Ficolin-2	FCN2	3.60
Complement factor H-related protein 1	CFHR1	3.35
Histidine-rich glycoprotein precursor	HRG	3.35
Desmoplakin I	DSP	3.35
Annexin A1	ANXA1	2.21
Alpha-1-antichymotrypsin	SERPINA3	2.21
Heat shock protein HSP 90-alpha	HSP90AA1	2.21
Spectrin beta chain, erythrocytic	SPTB	1.78
Thrombospondin-1	THBS1	1.49
Complement C1q subcomponent subunit C	C1QC	1.25
Immunoglobulin J chain	IGJ	1.11
Complement factor H	CFH	1.11
Fibrinogen beta chain	FGB	0.939
Band 3 anion transport protein	SLC4A1	0.905
Ankyrin-1	ANK1	0.848
Apolipoprotein A-I	APOA1	0.717
Alpha-2-macroglobulin	A2M	0.687
Immunoglobulin heavy constant mu	IGHM	0.676
CD5 antigen-like	CD5L	0.584
Hemopexin	HPX	0.542
Ig alpha-1 chain C region	IGHA1	0.449
Vitronectin	VTN	0.439
Actin, cytoplasmic 1	ACTB	0.420
Fibrinogen gamma chain	FGG	0.088
Ig gamma-2 chain C	IGHG2	0.087
Spectrin alpha chain, erythrocytic 1	SPTA1	0.048
Alpha-1-antitrypsin	SERPINA1	−0.033
Fibrinogen alpha chain	FGA	−0.113
Serum albumin	ALB	−0.394
Ficolin-3	FCN3	−0.454
Ceruloplasmin	CP	−0.477
Immunoglobulin kappa constant	IGKC	−0.497
Complement C1q subcomponent subunit A	C1QA	−0.647
Coagulation factor V	F5	−0.708
Pre-serum amyloid P component	APCS	−0.851
Haptoglobin	HP	−0.971
Complement C3	C3	−0.979
Ig lambda-2 chain C regions	IGLC2	−1.01
Erythrocyte band 7 integral membrane protein	STOM	−1.01
Inter-alpha-trypsin inhibitor heavy chain H1	ITIH1	−1.20
Serotransferrin	TF	−1.25
Inter-alpha-trypsin inhibitor heavy chain H2	ITIH2	−1.25
Inter-alpha-trypsin inhibitor heavy chain H4	ITIH4	−1.34
Complement C1q subcomponent subunit B	C1QB	−1.34
Complement component C4A	C4A	−2.33
Gelsolin	GSN	−2.44
Apolipoprotein B-100	APOB	−3.58

[a] R_{sc}, log 2 ratio between the protein expression levels in the corona of LF3-L *versus* LF3-S. Proteins in grey with $R_{sc} \geq 1.40$ or ≤ -1.40 were considered differentially represented.

Table 7 Quantitative proteomic analysis of PrC components for LF4-L *versus* LF4-S

Protein	Gene	R_{sc}[a]
Immunoglobulin heavy variable 3–66	IGHV3-66	3.64
Histidine-rich glycoprotein	HRG	3.64
Complement component C3	C3	3.64
Alpha-2-macroglobulin precursor	A2M	3.15
Fibrinogen alpha chain	FGA	1.73
Immunoglobulin kappa variable 3D-11	IGKV3D-11	1.32
Immunoglobulin kappa variable 3–20	IGKV3-20	1.12
Fibrinogen beta chain	FGB	0.951
Serum albumin	ALB	0.807
Immunoglobulin heavy constant mu	IGHM	0.491
Alpha-1-antitrypsin	SERPINA1	0.380
Fibrinogen gamma chain	FGG	0.295
Immunoglobulin kappa constant	IGKC	0.255
Vitronectin	VTN	−0.001
Complement C1q subcomponent subunit C	C1QC	−0.026
Ficolin-3	FCN3	−0.166
CD5 antigen-like	CD5L	−0.259
Ig alpha-1 chain C region	IGHA1	−0.441
Coagulation factor V	F5	−0.462
Ig gamma-2 chain C region	IGHG2	−0.581
Band 3 anion transport protein	SLC4A1	−1.19
Complement C1q subcomponent subunit A	C1QA	−1.30
Ig lambda-2 chain C regions	IGLC2	−1.35
Peroxiredoxin-2	PRDX2	−1.50
Apolipoprotein A-I	APOA1	−1.99
Thrombospondin-1	THBS1	−2.00
Ankyrin 1	ANK1	−2.36
Complement C1q subcomponent subunit B	C1QB	−2.46
Erythrocyte band 7 integral membrane protein	STOM	−2.65
Actin, cytoplasmic 1	ACTB	−2.89
Spectrin alpha chain, erythrocytic 1	SPTA1	−2.89
Spectrin beta chain, erythrocytic	SPTB	−3.28

[a] R_{sc}, log 2 ratio between the protein expression levels in the corona of LF4-L *versus* LF4-S. Proteins in grey with $R_{sc} \geq 1.40$ or ≤ -1.40 were considered differentially represented.

potential, meaning that higher contents correlated with lower zeta potential (Fig. 2c).

3.3. Functional classification of plasma proteins in the corona of LFs

The enrichment of Gene Ontology (GO) terms was performed on all the identified proteins to characterize them functionally according to Molecular Function (MF), Cellular Component (CC) and Biological Process (BP) categories (Table 3). The "immunoglobulin receptor binding" MF is the most represented GO term among the different LFs, except for LF5. Similarly, the most significant CC and BP categories included "fibrinogen complex" and "protein polymerization", being the PrCs highly enriched in fibrinogen proteins (Table 3). In line with previous findings,[12,77] fibrinogen and immunoglobulins mediate the opsonization phenomena, by which liposomes are marked to be eliminated by MPS. Interestingly, "complement activation" BP, to which opsonins belong, was not significantly represented in the coronas of PEGylated liposomes (Table 3), thus endorsing the anti-opsonization effect of PEG coating of NPs.[13] Accordingly, also apolipoproteins, another class of opsonin whose adsorption is able to modulate liposome biodistribution,[78] clustered in GO terms that are significantly represented in the coronas of PEG-free LFs (Table 3).

3.4. Differentially represented plasma proteins in the corona of LFs

Liposomes with the same formulation and different extrusion sizes. We performed MS-based label-free quantitative

Table 8 Quantitative proteomic analysis of PrC components for LF5-L *versus* LF5-S

Protein	Gene	R_{sc}[a]
Immunoglobulin kappa variable 2–30	IGKV2-30	3.12
Immunoglobulin heavy variable 3–72	IGHV3-72	2.91
Histidine-rich glycoprotein	HRG	2.67
Band 3 anion transport protein	SLC4A1	2.38
Immunoglobulin kappa variable 3–20	IGKV3-20	2.38
Fibrinogen alpha chain	FGA	2.38
Thrombospondin-1 precursor	THBS1	2.01
Plasma protease C1 inhibitor precursor	SERPING1	2.01
Coagulation factor V	F5	1.91
Alpha-2-HS-glycoprotein	AHSG	1.53
Complement factor H	CFH	1.53
Haptoglobin	HP	1.46
Apolipoprotein E	APOE	1.18
Fibrinogen gamma chain	FGG	0.757
Ig gamma-2 chain C region	IGHG2	0.693
Hemopexin	HPX	0.562
Immunoglobulin heavy constant mu	IGHM	0.440
Serum albumin	ALB	0.245
Alpha-2-macroglobulin	A2M	0.139
Vitronectin	VTN	0.123
Serotransferrin	TF	0.054
Zinc-alpha2-glycoprotein	AZGP1	0.053
Complement factor B	CFB	0.053
CD5 antigen-like	CD5L	−0.143
Inter-alpha-trypsin inhibitor heavy chain ITIH1	ITIH1	−0.180
Complement component C4A	C4A	−0.291
Fibrinogen beta chain	FGB	−0.301
Serum amyloid P-component	APCS	−0.311
Ficolin-3	FCN3	−0.443
Inter-alpha-trypsin inhibitor heavy chain H4	ITIH4	−0.495
Complement C1q subcomponent subunit B	C1QB	−0.525
Ig lambda-2 chain C regions	IGLC2	−0.531
Alpha-1-antitrypsin	SERPINA1	−0.564
Inter-alpha-trypsin inhibitor heavy chain H2	ITIH2	−0.640
Complement C1q subcomponent subunit C	C1QC	−0.657
Immunoglobulin kappa constant	IGKC	−0.694
Gelsolin	GSN	−0.797
Alpha-1-antichymotrypsin	SERPINA3	−0.798
Complement C3	C3	−0.932
Apolipoprotein A–I	APOA1	−1.63
Ceruloplasmin	CP	−1.77
Ig alpha-1 chain C region	IGHA1	−2.25
Ficolin-2	FCN2	−2.55
Apolipoprotein A-IV	APOA4	−3.12

[a] R_{SC}, log 2 ratio between the protein expression levels in the corona of LF5-L *versus* LF5-S. Proteins in grey with $R_{SC} \geq 1.40$ or ≤ -1.40 were considered differentially represented.

analysis using the spectral counting approach for protein abundance estimation. We compared the expression levels of identified plasma proteins between liposomes with the same formulation and different extrusion sizes: LFs-L *versus* LFs-S (Tables 4–8). Fifty unique proteins with $R_{sc} \geq 1.40$ or ≤ -1.40 were considered differentially represented in the corona of large and small LFs: 11 species for LF1, 19 for LF2, 13 for LF3, 14 for LF4 and 17 for LF5 (Tables 4–8). Among them, some proteins were formulation-specific, as reported in Fig. 3: 4 species for LF1, 10 for LF2, 6 for LF3, 6 for LF4 and 11 for LF5; in addition, their binding preferences in relation to the extrusion size are indicated in Fig. 3a. In particular, inter-alpha-trypsin inhibitor heavy chain H1, H2 and H4 (ITIH1, ITIH2, ITIH4) and vitamin D-binding protein (GC) were all LF1-specific proteins: the first three were over-represented in the corona of LF1-L *versus* LF1-S, whereas GC was under-represented within the same pairwise comparison. Among the ten differentially represented proteins in the corona of LF2-L *versus* LF2-S (Fig. 3a), those under-represented, such as ficolin-3 (FCN3), C4b-binding protein alpha chain (C4BPA), serum amyloid P-component (APCS) and FGB, and the over-represented ones, apolipoprotein L1 (APOL1) and immunoglobulin J chain (IGJ), were all significantly related to the biological process "innate immune response" (FDR = 0.0038) according to STRING analysis. Similarly, the "immune system" pathway was significantly enriched (FDR = 0.0024) among all the six LF3-specific differentially represented proteins (Fig. 3a). As for the over-represented proteins in the corona of LF4-L *versus* LF4-S, alpha-2-macroglobulin (A2M) and complement C3 (C3) were significantly related to the biological process "regulation of complement activation" (FDR = 0.0223), whereas the under-represented proteins, within the same pairwise comparison, did not cluster in any biological processes according to STRING analysis. Among LF5-specific differentially represented proteins, only complement factor H (CFH), plasma protease C1 inhibitor precursor (SERPING1) and coagulation factor V (F5) significantly clustered in the "complement and coagulation cascades" pathway (FDR = 0.00076): all these three proteins were over-represented in the corona of LF5-L *versus* LF5-S (Fig. 3a). Overall, these results strengthen the evidence of the role that the NP size plays in determining preferential adsorption of specific proteins on the liposome surface as well as their relative abundance in the PrC.

Moreover, other proteins were found in PrC as common species to at least three LFs as reported in the Venn diagram of Fig. 3a; their binding preferences (LFs-L *versus* LFs-S) are shown in Fig. 3b. For example, thrombospondin-1 (THBS1) was shared by all the LFs; whereas spectrin beta chain, erythrocytic (SPTB) by all LFs except for GM1-coated LFs and ankyrin-1 (ANK1) only by PEG-free LFs (LF1 and LF2) and PEGylated LF4. Interestingly, all these common proteins were, in general, over-represented in LFs-L *versus* LFs-S except for PEGylated LF4 (Fig. 3b).

Liposomes with the same extrusion size and different formulations. We also compared the expression levels of identified plasma proteins among liposomes with the same extrusion size (100 nm or 200 nm) and different LFs. In the ESI Tables S6 and S7,† R_{sc} values of ten pairwise comparisons are reported for each identified protein in the corona of either all LFs-L or LFs-S, respectively. To point out groups of proteins sharing common and/or specific patterns in terms of relative abundance in the PrC of the different LFs, we generated heatmap views based on the R_{sc} values (ESI Fig. S3a and b† for LFs-L and LFs-S, respectively). Interestingly, several proteins showed the same expression trends in all the possible pairwise comparisons (ESI Table S8†). However, the clustering highlighted different patterns between the two heatmap views (ESI Fig. S3a and b†).

Among the investigated LFs, PEG- and GM1-bearing LFs (LF3–5) are suitable NPs for applications of *in vivo* delivery in

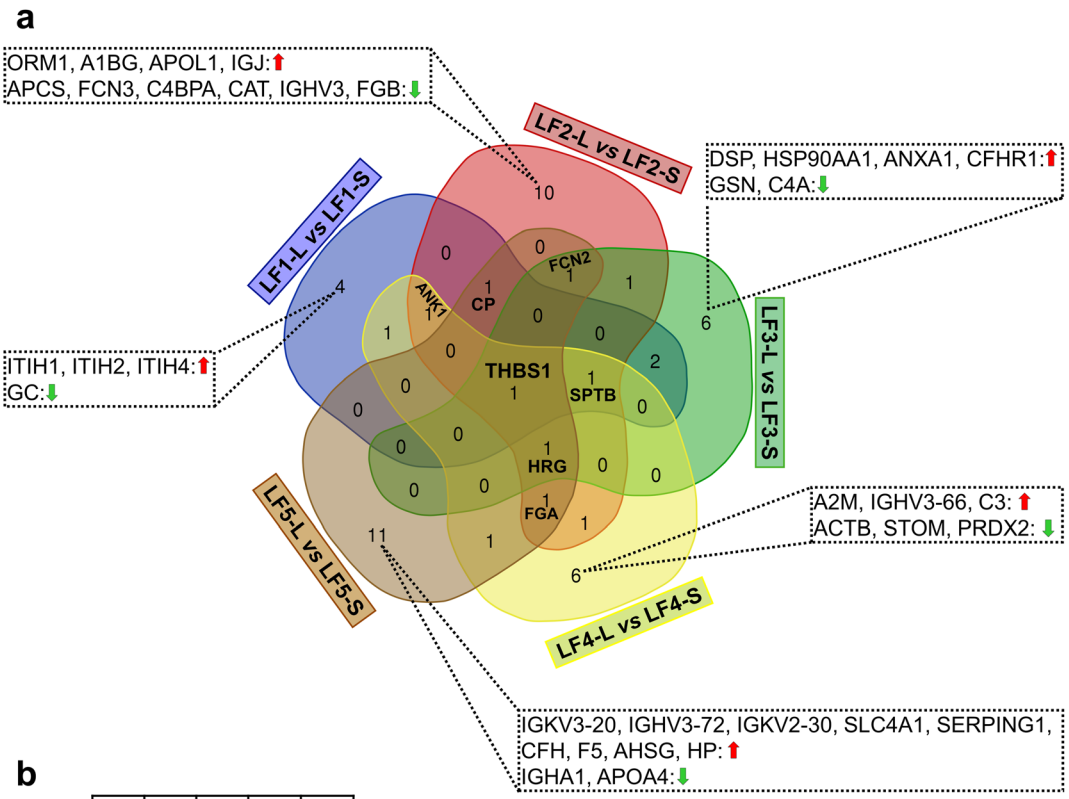

b

	LF1	LF2	LF3	LF4	LF5
THBS1	⬆	⬆	⬆	⬇	⬆
HRG	/	⬆	⬆	⬆	⬆
ANK1	⬆	⬆	/	⬇	n.d.
SPTB	⬆	⬆	⬆	⬇	n.d.
CP	⬆	⬆	/	n.d.	⬇
FCN2	/	⬇	⬆	n.d.	⬇
FGA	/	⬇	/	⬆	⬆

Fig. 3 Venn diagram of differentially represented proteins in the corona. (a) Venn diagram shows the over-represented (red arrow) and under-represented (green arrow) proteins specific for each of the five pairwise comparisons (listed in the box) and those common to at least three pairwise comparisons. (b) Within each pairwise comparison, proteins shared by LFs were reported together with their differential representation (LFs-L *versus* LFs-S). Only proteins with R_{sc} of ≥1.40 or ≤−1.40 were included in the diagram. n.d. = not determined (the protein was not identified in both LF-L and LF-S formulations); / = below the threshold, *i.e.*, R_{sc} < 1.40 or >−1.40.

terms of extended circulation time and immune/reticuloendothelial system avoidance;[79–82] moreover, GM1-NPs are also able to overcome the brain barrier (BBB).[83,84] Hence, we pointed out the composition-specific patterns shared by small and large LF5 in comparison with the corresponding PEGylated LFs (Fig. 4a).

Interestingly, the comparison between LF5 and LF3/LF4 corona allowed us to identify two dense groups of proteins, termed cluster 1 and cluster 2, which showed a marked opposite NP-binding preference (Fig. 4a). In fact, cluster 1 proteins preferentially bind PEGylated liposomes (LF3 and LF4), while cluster 2 proteins preferentially adsorb onto GM1 liposomes (LF5). The trends of relative abundance of cluster 1 and 2 proteins are highlighted by a profile plot analysis in Fig. 4a, left inserts. A magnification of these profile plots, including protein names, is shown in ESI Fig. S4.†

Cluster 1 is constituted by 7 proteins, namely erythrocyte band 7 integral membrane protein (STOM), peroxiredoxin-2 (PRDX2), SLC4A1, THBS1, SPTB, spectrin alpha chain, erythrocytic 1 (SPTA1), ANK1, and is more represented in the PrC of PEGylated LFs (LF3 and LF4) than in GM1-incorporating ones (LF5). All these proteins, except THBS1, cluster together, as revealed by STRING analysis (Fig. 4b). Among them, SLC4A1, SPTB, SPTA1, and ANK1 physically interact with each other. Interestingly, similar proteins were identified *in vitro* and *in vivo* in the PrC of PEGylated formulations, enforcing a putative role of these species in the nano-bio interfaces between HuP and NPs.[18,85,86] However, the effects of such corona proteins remain to be understood. As for THBS1, this secreted glycoprotein interacts with components of the extracellular matrix and various cell surface receptors. It is present in plasma, acting as a regulator of blood pressure and hemostasis, and it also plays roles in regulating immune responses. THBS1 can bridge phagocytic immune cells with other cell types, including platelets and apoptotic cells, thereby promoting the activity of professional phagocytic cells.[87] Hence, we may speculate that

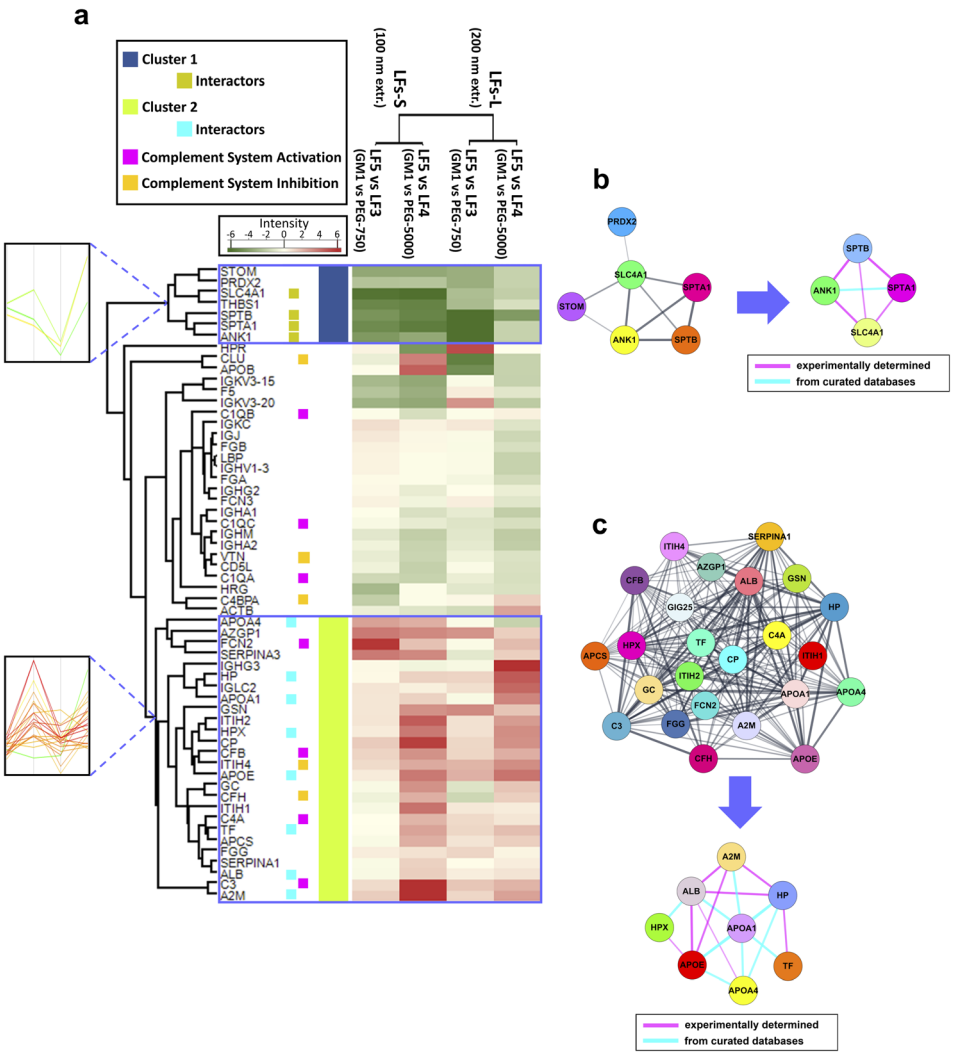

Fig. 4 Proteomic and functional characterization of GM1-incorporating LFs. (a) Heatmap visualization of corona protein relative abundance of LF5-S and LF5-L (GM1-LFs at 100 nm and 200 nm extrusion, respectively) in comparison with LF3 (PEG750-LFs) or LF4 (PEG5000-LFs). Protein abundance based on R_{sc} is reported as color intensity ranging from green to red. Two clusters were identified, namely cluster 1 and cluster 2, with marked opposite NP-binding preference. Profile plots of the selected clusters are also highlighted (left inserts) (a magnification of these profile plots is contained in ESI Fig. S3,† where most of the protein names are also indicated). Functional annotation was reported for selected proteins in the heatmap. (b and c) Results of protein–protein interaction networks retrieved by STRING analysis for the proteins of cluster 1 and 2, respectively. From each of the two networks, subnetworks were generated to highlight the species known to physically interact with each other. The thickness of edges (connecting lines) is proportional to interaction confidence.

the presence of this protein on the NP surface might enhance the MPS clearance. Here, THBS1, as the other cluster1 proteins, preferentially binds LF3 and LF4 rather than LF5, suggesting that the supposed enhanced phagocytic effect could be higher in PEGylated LFs than in GM1 LFs. Moreover, THBS1 showed size-dependent differential binding with all the LFs (Fig. 3a and b), and it is more represented in the corona of LFs-L than LFs-S, except in the case of LF4 (bearing long PEG chains). This additional result could imply that the phagocytic effect could be higher for LF-L that for LF-S, except for high MW PEGylated liposomes.

Cluster 2 is comprised of 26 proteins, of which 24 species cluster together upon STRING analysis (Fig. 4c). Among them, 6 proteins are regulators or factors of the complement system (ficolin-2, FCN2, complement factor B, CFB, ITIH4, complement factor H, CFH, complement C4-A, C4A, C3).[71,88] In addition, within Cluster 2, apolipoprotein A-IV (APOA4), HP, apolipoprotein A–I (APOA1), hemopexin (HPX), apolipoprotein E (APOE), TF, ALB, and A2M constitute a network of interacting species (Fig. 4c), suggesting a possible mechanism of cooperative adsorption of proteins.[89,90]

Some proteins belonging to cluster 2 have been previously reported in PrC studies and here they are shared by most of the investigated LFs (Table 2). In fact, besides ALB, whose functions as NP components are well-known,[18,74] TF, APOE and APOA1 are used to functionalize liposomes or other NPs for active targeting. Conjugation of NPs with TF is extensively used for drug delivery purposes since such strategy exploits the ability to specifically bind to transferrin receptors (TFR); in fact, many types of tumor cells and endothelial cells over-express TFR,

thereby allowing TF-conjugated NPs to take advantage of TFR-mediated endocytosis.[91] Indeed, liver cells highly overexpress TFRs[92] and, recently, TF-conjugated liposomes were used to effectively target liver cancer.[93] However, a large body of evidence indicates that TF-functionalized liposomes are particularly effective for blood–brain barrier (BBB) targeting and drug delivery to the central nervous system (CNS)[94–96] since TFRs are abundant on the plasmatic membrane of brain endothelial cells and neurons.[95,96]

APOE and APOA1 apolipoproteins are considered (together with ALB) dysopsonins[78,89] that can inhibit monocyte uptake[74] and confer stealth properties to NPs.[97] As part of the delicate balance between opsonins and dysopsonins that determine the fate of NPs,[78] the preferential presence on the LF5 corona of APOE and APOA1, together with ALB, could represent a molecular label that potentially makes GM1-liposomes more suitable than PEG-liposomes for drug delivery applications. Interestingly, APOE conjugation with liposomes is widely used as a means to enhance delivery to the CNS[98–100] and liver.[101] In fact, APOE functions as a ligand for low density lipoprotein (LDL) receptors (LDLR) that are expressed at high levels by normal and tumoral hepatocytes, brain endothelial cells and neuronal cells.[98] The presence of APOE on the surface of NPs enhances the ability to overcome the BBB through LDLR-mediated transcytosis/endocytosis, thereby favoring the accumulation of NPs or their payload to brain tumors.[98]

APOA1 is a main protein constituent of high-density lipoprotein (HDL) and can actively bind to HDL receptors and mainly to scavenger receptor type I (SR-B1), which are highly expressed on the membrane of hepatocytes.[102,103] For this reason, APOA1-conjugated liposomes/NPs have been widely adopted in liver-targeted drug delivery strategies.[102,103]

Taken together, the co-presence of TF, APOE and APOA1 on the PrC of GM1-containing liposomes could be a signature characterizing NPs able to target specific tissues, such as the brain and the liver.

4. Conclusions

This study consisted of a formulation/size-based multiplexed mapping of PrC composition that allowed us to highlight (i) the common as well as the unique species for all formulations; (ii) the correlation between each identified corona protein and various physicochemical properties (size, PDI or zeta potential); (iii) some preferential binding determined by the size within the same formulation, or by the formulation within the two extrusion sizes; (iv) the striking different corona composition between PEG- and GM1-containing LFs. In fact, we identified two clusters of plasma proteins with a preferential binding to PEG-containing liposomes (cluster 1) or GM1-containing formulations (cluster 2).

Currently, some authors recognize it as instrumental to distinguish protein patterns within PrC constituted by a quali-quantitative variety of species organized in a sort of multifaceted protein domains. These may represent a structural/functional tridimensional scaffold motif that mediates cell targeting and uptake.[36,37] In agreement with the novel concept of bionanosynapsis, representing the interaction between PrC-NPs and biological tissues able to trigger a cellular response,[36,37] we suggest cluster 1 and 2 as multifaceted protein domains that specifically contribute to the novel biological identity of PEG- and GM1-coated liposomes, respectively.

The results obtained in this work take into account the possibility of controlling the PrC composition by modulating physicochemical properties and tuning surface features of LFs to the possible future aim of targeting active molecules to the specific tissue of action. Investigating clusters in PrC will help to decode the multivalent roles of the protein pattern components in the drug delivery process, taking advantage of the bionanoscale recognition and identity for significant advances in nanomedicine.

However, to reach such future progress, there is an urgent need for innovative approaches, including the implementation of artificial intelligence and machine learning algorithms aimed at disentangling the heterogeneous composition of NP coronas, such as the metabolite corona.[104,105] Indeed, the low molecular weight metabolites may further influence the bionano interactions, and hence, other specific biological insights.

Author contributions

CC, EI, LDM, SO: conceptualization, methodology, investigation, writing the original draft. FS and MF: overall supervision and project planning and administration, writing, editing, and revision. CC, LDM and NdA performed the experiments for the synthesis and physicochemical characterization of liposomes, analyzed the resulting data and discussed the relative results. EI performed proteomic analyses. EI, AC and MC analyzed the proteomic data, performed bioinformatic analyses and correlations, and discussed the relative results. SO supervised proteomic and bioinformatic analyses. FS and MF drafted and supervised the editing of the manuscript and critically revised the results and the whole content of the paper. All the authors participated in the writing and revision of the manuscript.

Data availability

The data supporting this article have been included as part of the ESI.† The mass spectrometry proteomics data have been deposited to the ProteomeXchange Consortium *via* the PRIDE partner repository[46] with the dataset identifier PXD052701.

Conflicts of interest

All authors declare no conflict of interest.

Acknowledgements

This work was supported by: Ministero della Salute [RF-2010-23183729] to F. S.; Grants from Regione Campania [CIRO project: infrastructures and scientific instrumentation to CEINGE (Coordinator: Prof. Francesco Salvatore) D. D. n.366/2018; SATIN "Neoplasia studies" POR Campania FESR 2014/2020; D. D. Regione Campania n.459/2018; "Predictive

Medicine in neoplasia", L. Regione Campania n.752/2019 and n.38/2020; "Studi sulla Lotta alle Malattie Neoplastiche" (BURC: L.752/2019; Legge n.38/2020 art.16, D. D. Regione Campania n.48/2021; D. D. Regione Campania n.359/2022; D. D. Regione Campania n.9/2023)] all to F. S.; Ministero dell'Università e della Ricerca (MUR) [FAR 2018 (D56C18000780005), FAR 2019 (D54I19002790005)]; the European Union – NextGenerationEU, under the National Recovery and Resilience Plan (NRRP), Mission 4 Component 2 – M4C2, Investment 1.5 – Call for tender No. 3277 of 30.12.2021, Italian Ministry of University, Award Number: ECS00000041, Project Title: "Innovation, digitalization and sustainability for the diffused economy in Central Italy", Concession Degree No. 1057 of 23.06.2022 adopted by the Italian Ministry of University. CUP: D73C22000840006 (grant holder: Luisa Di Marzio and Christian Celia); Overseas Visiting Fellow Program 2022, University of Shanghai, China (grant holder: Christian Celia). We are grateful to Jean Ann Gilder (Scientific Communication s.r.l., Naples, Italy), a native English expert, for editing the text language.

References

1 E. Beltrán-Gracia, A. López-Camacho, I. Higuera-Ciapara, J. B. Velázquez-Fernández and A. A. Vallejo-Cardona, *Cancer Nanotechnol.*, 2019, **10**, 11.
2 G. Bozzuto and A. Molinari, *Int. J. Nanomed.*, 2015, 975.
3 H. Nsairat, D. Khater, U. Sayed, F. Odeh, A. Al Bawab and W. Alshaer, *Heliyon*, 2022, **8**, e09394.
4 X. Wang, F. Wang, S. Li, G. Yin and X. Pu, *Curr. Drug Delivery*, 2022, **19**, 940–948.
5 F. Gong, Z. Wang, R. Mo, Y. Wang, J. Su, X. Li, C. T. Q. Omonova, A. M. Khamis, Q. Zhang, M. Dong and Z. Su, *J. Controlled Release*, 2022, **349**, 940–953.
6 T. Shehata, K. Ogawara, K. Higaki and T. Kimura, *Int. J. Pharm.*, 2008, **359**, 272–279.
7 A. Akbarzadeh, R. Rezaei-Sadabady, S. Davaran, S. W. Joo, N. Zarghami, Y. Hanifehpour, M. Samiei, M. Kouhi and K. Nejati-Koshki, *Nanoscale Res. Lett.*, 2013, **8**, 102.
8 K. Yang, K. Tran and A. Salvati, *Biomolecules*, 2022, **13**, 59.
9 T. M. Allen and P. R. Cullis, *Adv. Drug Delivery Rev.*, 2013, **65**, 36–48.
10 Y. Takakura and Y. Takahashi, *J. Controlled Release*, 2022, **350**, 486–493.
11 C. Corbo, R. Molinaro, A. Parodi, N. E. Toledano Furman, F. Salvatore and E. Tasciotti, *Nanomedicine*, 2016, **11**, 81–100.
12 F. Giulimondi, L. Digiacomo, D. Pozzi, S. Palchetti, E. Vulpis, A. L. Capriotti, R. Z. Chiozzi, A. Laganà, H. Amenitsch, L. Masuelli, G. Peruzzi, M. Mahmoudi, I. Screpanti, A. Zingoni and G. Caracciolo, *Nat. Commun.*, 2019, **10**, 3686.
13 S. Palchetti, V. Colapicchioni, L. Digiacomo, G. Caracciolo, D. Pozzi, A. L. Capriotti, G. La Barbera and A. Laganà, *Biochim. Biophys. Acta, Biomembr.*, 2016, **1858**, 189–196.
14 A. Cevenini, C. Celia, S. Orrù, D. Sarnataro, M. Raia, V. Mollo, M. Locatelli, E. Imperlini, N. Peluso, R. Peltrini, E. De Rosa, A. Parodi, L. Del Vecchio, L. Di Marzio, M. Fresta, P. A. Netti, H. Shen, X. Liu, E. Tasciotti and F. Salvatore, *Pharmaceutics*, 2020, **12**, 559.
15 Y. Gao, M. Joshi, Z. Zhao and S. Mitragotri, *Bioeng. Transl. Med.*, 2023, **9**, e10600.
16 N. D'Avanzo, C. Celia, A. Barone, M. Carafa, L. Di Marzio, H. A. Santos and M. Fresta, *Adv. Ther.*, 2020, **3**, 1900170.
17 E. Tasciotti, R. Molinaro, F. Taraballi, N. Toledano Furman, M. Sherman, A. Parodi, F. Salvatore and C. Corbo, *Int. J. Nanomed.*, 2016, **11**, 3049–3063.
18 E. Imperlini, C. Celia, A. Cevenini, A. Mandola, M. Raia, M. Fresta, S. Orrù, L. Di Marzio and F. Salvatore, *Nanoscale*, 2021, **13**, 5251–5269.
19 S. Yang, Y. Liu, Y. Wang and A. Cao, *Small*, 2013, **9**, 1635–1653.
20 M. Zhu, G. Nie, H. Meng, T. Xia, A. Nel and Y. Zhao, *Acc. Chem. Res.*, 2013, **46**, 622–631.
21 T. Cedervall, I. Lynch, M. Foy, T. Berggård, S. C. Donnelly, G. Cagney, S. Linse and K. A. Dawson, *Angew. Chem., Int. Ed.*, 2007, **46**, 5754–5756.
22 M. P. Monopoli, D. Walczyk, A. Campbell, G. Elia, I. Lynch, F. Baldelli Bombelli and K. A. Dawson, *J. Am. Chem. Soc.*, 2011, **133**, 2525–2534.
23 L. Vroman, *Nature*, 1962, **196**, 476–477.
24 S. Milani, F. Baldelli Bombelli, A. S. Pitek, K. A. Dawson and J. Rädler, *ACS Nano*, 2012, **6**, 2532–2541.
25 E. Mahon, A. Salvati, F. Baldelli Bombelli, I. Lynch and K. A. Dawson, *J. Controlled Release*, 2012, **161**, 164–174.
26 L. Wang, J. Li, J. Pan, X. Jiang, Y. Ji, Y. Li, Y. Qu, Y. Zhao, X. Wu and C. Chen, *J. Am. Chem. Soc.*, 2013, **135**, 17359–17368.
27 M. Kendall, P. Ding and K. Kendall, *Nanotoxicology*, 2011, **5**, 55–65.
28 M. A. Wells, A. Abid, I. M. Kennedy and A. I. Barakat, *Nanotoxicology*, 2012, **6**, 837–846.
29 K. Yang, B. Mesquita, P. Horvatovich and A. Salvati, *Acta Biomater.*, 2020, **106**, 314–327.
30 M. Pannuzzo, S. Esposito, L.-P. Wu, J. Key, S. Aryal, C. Celia, L. di Marzio, S. M. Moghimi and P. Decuzzi, *Nano Lett.*, 2020, **20**, 4312–4321.
31 L. Wei, D. Zhao, W. Sun, L. Lin, D. Sui, W. Li, Y. Gui, J. Wang, Y. Deng and Y. Song, *Eur. J. Pharm. Biopharm.*, 2023, **184**, 50–61.
32 M. L. Immordino, F. Dosio and L. Cattel, *Int. J. Nanomed.*, 2006, **1**, 297–315.
33 S. Arumugam, S. Schmieder, W. Pezeshkian, U. Becken, C. Wunder, D. Chinnapen, J. H. Ipsen, A. K. Kenworthy, W. Lencer, S. Mayor and L. Johannes, *Nat. Commun.*, 2021, **12**, 3675.
34 J. W. Shreffler, J. E. Pullan, K. M. Dailey, S. Mallik and A. E. Brooks, *Int. J. Mol. Sci.*, 2019, **20**(23), 6056.
35 L. Wang, X. Ji, D. Guo, C. Shi and J. Luo, *Mol. Pharm.*, 2021, **18**, 2349–2359.
36 M. Mahmoudi, M. P. Landry, A. Moore and R. Coreas, *Nat. Rev. Mater.*, 2023, **8**, 422–438.
37 K. A. Dawson and Y. Yan, *Nat. Nanotechnol.*, 2021, **16**, 229–242.

38 J. Wolfram, B. Scott, K. Boom, J. Shen, C. Borsoi, K. Suri, R. Grande, M. Fresta, C. Celia, Y. Zhao, H. Shen and M. Ferrari, *Curr. Drug Delivery*, 2016, **13**, 711–719.
39 G. N. Roviello, G. Roviello, D. Musumeci, D. Capasso, S. Di Gaetano, M. Costanzo and C. Pedone, *RSC Adv.*, 2014, **4**, 28691–28698.
40 E. Imperlini, I. Colavita, M. Caterino, P. Mirabelli, D. Pagnozzi, L. Del Vecchio, R. Di Noto, M. Ruoppolo and S. Orrù, *J. Cell. Biochem.*, 2013, **114**, 2577–2587.
41 E. Imperlini, A. Mancini, S. Spaziani, D. Martone, A. Alfieri, M. Gemei, L. Del Vecchio, P. Buono and S. Orrù, *Proteomics*, 2010, **10**, 3165–3175.
42 M. Costanzo, M. Caterino, A. Cevenini, L. Kollipara, O. Shevchuk, C. D. L. Nguyen, A. Sickmann and M. Ruoppolo, in *NATO Science for Peace and Security Series A: Chemistry and Biology*, Springer Science and Business Media B.V., 2020, pp. 221–223.
43 M. Costanzo, A. Cevenini, L. Kollipara, M. Caterino, S. Bianco, F. Pirozzi, G. Scerra, M. D'Agostino, L. M. Pavone, A. Sickmann and M. Ruoppolo, *Cell Biosci.*, 2024, **14**, 63.
44 E. Imperlini, S. Orrù, C. Corbo, A. Daniele and F. Salvatore, *J. Neurochem.*, 2014, **129**, 1002–1012.
45 F. Prisco, D. De Biase, G. Piegari, F. Oriente, I. Cimmino, V. De Pasquale, M. Costanzo, P. Santoro, M. Gizzarelli, S. Papparella and O. Paciello, *Pathogens*, 2021, **10**, 463.
46 Y. Perez-Riverol, J. Bai, C. Bandla, D. García-Seisdedos, S. Hewapathirana, S. Kamatchinathan, D. J. Kundu, A. Prakash, A. Frericks-Zipper, M. Eisenacher, M. Walzer, S. Wang, A. Brazma and J. A. Vizcaíno, *Nucleic Acids Res.*, 2022, **50**, D543–D552.
47 D. Drongitis, M. Caterino, L. Verrillo, P. Santonicola, M. Costanzo, L. Poeta, B. Attianese, A. Barra, G. Terrone, M. B. Lioi, S. Paladino, E. Di Schiavi, V. Costa, M. Ruoppolo and M. G. Miano, *Hum. Mol. Genet.*, 2022, **31**, 1884–1908.
48 B. T. Sherman, M. Hao, J. Qiu, X. Jiao, M. W. Baseler, H. C. Lane, T. Imamichi and W. Chang, *Nucleic Acids Res.*, 2022, **50**, W216–W221.
49 V. Manganelli, I. Salvatori, M. Costanzo, A. Capozzi, D. Caissutti, M. Caterino, C. Valle, A. Ferri, M. Sorice, M. Ruoppolo, T. Garofalo and R. Misasi, *Cells*, 2021, **10**, 3394.
50 M. Costanzo, M. Caterino, A. Cevenini, V. Jung, C. Chhuon, J. Lipecka, R. Fedele, I. C. Guerrera and M. Ruoppolo, *Data Brief*, 2020, **33**, 106453.
51 M. Costanzo, M. Caterino, I. Salvatori, V. Manganelli, A. Ferri, R. Misasi and M. Ruoppolo, *Data Brief*, 2022, **41**, 107843.
52 M. Gonzalez Melo, A. O. Fontana, D. Viertl, G. Allenbach, J. O. Prior, S. Rotman, R. G. Feichtinger, J. A. Mayr, M. Costanzo, M. Caterino, M. Ruoppolo, O. Braissant, F. Barbey and D. Ballhausen, *Mol. Genet. Metab.*, 2021, **134**, 287–300.
53 L. Santorelli, M. Caterino and M. Costanzo, *OMICS: J. Integr. Biol.*, 2022, **26**, 633–649.
54 E. Quagliarini, L. Digiacomo, S. Renzi, D. Pozzi and G. Caracciolo, *Nano Today*, 2022, **47**, 101657.
55 W. Fan, H. Peng, Z. Yu, L. Wang, H. He, Y. Ma, J. Qi, Y. Lu and W. Wu, *Acta Pharm. Sin. B*, 2022, **12**, 2479–2493.
56 B.-M. Chen, T.-L. Cheng and S. R. Roffler, *ACS Nano*, 2021, **15**, 14022–14048.
57 C. Finsterwald, S. Dias, P. J. Magistretti and S. Lengacher, *Front. Pharmacol.*, 2021, **12**, 653842.
58 A. Benady, D. Freidin, C. G. Pick and V. Rubovitch, *Sci. Rep.*, 2018, **8**, 13340.
59 InnoMedica Schweiz AG and Bern, Svizzera, Safety Evaluation of Intravenous Talineuren (TLN) in Parkinson's Disease-affected Patients, ClinicalTrials.gov ID: NCT04976127, 2021, **https://www.clinicaltrials.gov/study/NCT04976127?term=Talineuren&rank=1**.
60 N. d'Avanzo, D. Paolino, A. Barone, L. Ciriolo, A. Mancuso, M. C. Christiano, A. M. Tolomeo, C. Celia, X. Deng and M. Fresta, *Drug Delivery Transl. Res.*, 2024, DOI: **10.1007/s13346-024-01556-3**.
61 D. Prasad and K. Muniyappa, *Biochemistry*, 2019, **58**, 1295–1310.
62 J. Morgenstern, P. Baumann, C. Brunner and J. Hubbuch, *Int. J. Pharm.*, 2017, **519**, 408–417.
63 K. Abe, K. Higashi, K. Watabe, A. Kobayashi, W. Limwikrant, K. Yamamoto and K. Moribe, *Colloids Surf., A*, 2015, **474**, 63–70.
64 P. Resnier, E. Lepeltier, A. L. Emina, N. Galopin, J. Bejaud, S. David, C. Ballet, T. Benvegnu, F. Pecorari, I. Chourpa, J.-P. Benoit and C. Passirani, *RSC Adv.*, 2019, **9**, 27264–27278.
65 A. Mori, A. L. Klibanov, V. P. Torchilin and L. Huang, *FEBS Lett.*, 1991, **284**, 263–266.
66 P. Grad, L. Gedda and K. Edwards, *J. Colloid Interface Sci.*, 2020, **578**, 281–289.
67 M. E. Haque and B. R. Lentz, *Biochemistry*, 2004, **43**, 3507–3517.
68 E. Jaradat, E. Weaver, A. Meziane and D. A. Lamprou, *Mol. Pharm.*, 2023, **20**, 6184–6196.
69 G. Pasut and F. M. Veronese, *J. Controlled Release*, 2012, **161**, 461–472.
70 A. A. Sebak, I. E. O. Gomaa, A. N. ElMeshad, M. H. Farag, U. Breitinger, H.-G. Breitinger and M. H. AbdelKader, *Int. J. Nanomed.*, 2020, **15**, 9539–9556.
71 D. Ricklin, G. Hajishengallis, K. Yang and J. D. Lambris, *Nat. Immunol.*, 2010, **11**, 785–797.
72 M. Chen, M. Ding, Y. Li, X. Zhong, S. Liu, Z. Guo, X. Yin, S. Fu and J. Ye, *Dev. Comp. Immunol.*, 2018, **87**, 98–108.
73 P. T. Gomme, K. B. McCann and J. Bertolini, *Drug Discovery Today*, 2005, **10**, 267–273.
74 R. Wang, Z. Zhang, B. Liu, J. Xue, F. Liu, T. Tang, W. Liu, F. Feng and W. Qu, *Biomater. Sci.*, 2021, **9**, 3621–3637.
75 H. Li and Z. M. Qian, *Med. Res. Rev.*, 2002, **22**, 225–250.
76 M. R. Sepand, M. Ghavami, S. Zanganeh, S. Stacks, F. Ghasemi, H. Montazeri, C. Corbo, H. Derakhshankhah, S. N. Ostad, M. H. Ghahremani and M. Mahmoudi, *Nanoscale*, 2020, **12**, 4935–4944.

77 O. K. Kari, J. Ndika, P. Parkkila, A. Louna, T. Lajunen, A. Puustinen, T. Viitala, H. Alenius and A. Urtti, *Nanoscale*, 2020, **12**, 1728–1741.
78 E. Papini, R. Tavano and F. Mancin, *Front. Immunol.*, 2020, **11**, 567365.
79 D. Liu, Q. Hu and Y. K. Song, *Biochim. Biophys. Acta, Biomembr.*, 1995, **1240**, 277–284.
80 E. Nogueira, A. Loureiro, P. Nogueira, J. Freitas, C. R. Almeida, J. Härmark, H. Hebert, A. Moreira, A. M. Carmo, A. Preto, A. C. Gomes and A. Cavaco-Paulo, *Faraday Discuss.*, 2013, **166**, 417.
81 J. S. Suk, Q. Xu, N. Kim, J. Hanes and L. M. Ensign, *Adv. Drug Delivery Rev.*, 2016, **99**, 28–51.
82 H. B. Haroon, A. C. Hunter, Z. S. Farhangrazi and S. M. Moghimi, *Adv. Drug Delivery Rev.*, 2022, **188**, 114396.
83 D. Zou, W. Wang, D. Lei, Y. Yin, P. Ren, J. Chen, T. Yin, B. Wang, G. Wang and Y. Wang, *Int. J. Nanomed.*, 2017, **12**, 4879–4889.
84 M. Mora, M.-L. Sagristá, D. Trombetta, F. P. Bonina, A. De Pasquale and A. Saija, *Pharm. Res.*, 2002, **19**, 1430–1438.
85 M. Hadjidemetriou, S. McAdam, G. Garner, C. Thackeray, D. Knight, D. Smith, Z. Al-Ahmady, M. Mazza, J. Rogan, A. Clamp and K. Kostarelos, *Adv. Mater.*, 2019, **31**, e1803335.
86 M. Hadjidemetriou, Z. Al-Ahmady, M. Mazza, R. F. Collins, K. Dawson and K. Kostarelos, *ACS Nano*, 2015, **9**, 8142–8156.
87 S. Kaur and D. D. Roberts, *Semin. Cell Dev. Biol.*, 2024, **155**, 22–31.
88 R. Pihl, R. K. Jensen, E. C. Poulsen, L. Jensen, A. G. Hansen, I. B. Thøgersen, J. Dobó, P. Gál, G. R. Andersen, J. J. Enghild and S. Thiel, *Sci. Adv.*, 2021, **7**, eaba7381.
89 S. Panico, S. Capolla, S. Bozzer, G. Toffoli, M. Dal Bo and P. Macor, *Pharmaceutics*, 2022, **14**, 2605.
90 R. L. Pinals, D. Yang, D. J. Rosenberg, T. Chaudhary, A. R. Crothers, A. T. Iavarone, M. Hammel and M. P. Landry, *Angew. Chem., Int. Ed.*, 2020, **59**, 23668–23677.
91 H. Iqbal, T. Yang, T. Li, M. Zhang, H. Ke, D. Ding, Y. Deng and H. Chen, *J. Controlled Release*, 2021, **329**, 997–1022.
92 S. Li, H. Zhao, X. Mao, Y. Fan, X. Liang, R. Wang, L. Xiao, J. Wang, Q. Liu and G. Zhao, *Pharm. Res.*, 2019, **36**, 168.
93 A. Yang, Z. Sun, R. Liu, X. Liu, Y. Zhang, Y. Zhou, Y. Qiu and X. Zhang, *Front. Oncol.*, 2021, **11**, 727605.
94 T. Koneru, E. McCord, S. Pawar, K. Tatiparti, S. Sau and A. K. Iyer, *ACS Omega*, 2021, **6**, 8727–8733.
95 S. Andrade, M. J. Ramalho, J. A. Loureiro and M. C. Pereira, *Int. J. Pharm.*, 2022, **626**, 122167.
96 S. Andrade, J. A. Loureiro and M. C. Pereira, *Pharmaceutics*, 2022, **14**, 2163.
97 R. Bilardo, F. Traldi, A. Vdovchenko and M. Resmini, *Wiley Interdiscip. Rev.: Nanomed. Nanobiotechnol.*, 2022, **14**, e1788.
98 M. Ismail, W. Yang, Y. Li, T. Chai, D. Zhang, Q. Du, P. Muhammad, S. Hanif, M. Zheng and B. Shi, *Biomaterials*, 2022, **287**, 121608.
99 Y.-C. Kuo, I.-W. Ng and R. Rajesh, *Mater. Sci. Eng., C*, 2021, **127**, 112233.
100 N. Grafals-Ruiz, C. I. Rios-Vicil, E. L. Lozada-Delgado, B. I. Quiñones-Díaz, R. A. Noriega-Rivera, G. Martínez-Zayas, Y. Santana-Rivera, G. S. Santiago-Sánchez, F. Valiyeva and P. E. Vivas-Mejía, *Int. J. Nanomed.*, 2020, **15**, 2809–2828.
101 P. Dalhaimer, B. Florey and S. Isaac, *ACS Nano*, 2023, **17**, 837–842.
102 W. Xu, Y. Niu, X. Ai, C. Xia, P. Geng, H. Zhu, W. Zhou, H. Huang and X. Shi, *Biomedicines*, 2022, **10**, 900.
103 R. Kuai, D. Li, Y. E. Chen, J. J. Moon and A. Schwendeman, *ACS Nano*, 2016, **10**, 3015–3041.
104 G. J. Jang, J. Y. Jeong, H. Joung and S. Y. Han, *Colloids Surf., B*, 2023, **230**, 113488.
105 A. J. Chetwynd, W. Zhang, J. A. Thorn, I. Lynch and R. Ramautar, *Small*, 2020, **16**, e2000295.